

# Neutron skin thickness and its volume and surface contributions

Peng Wang,<sup>1</sup> Zi-Dan Huang,<sup>1</sup> Shuang-Quan Zhang,<sup>2</sup> and Ting-Ting Sun<sup>1,\*</sup>

<sup>1</sup>*School of Physics, Zhengzhou University, Zhengzhou 450001, China*

<sup>2</sup>*State Key Laboratory of Nuclear Physics and Technology,  
School of Physics, Peking University, Beijing 100871, China*

Accurate determination of the neutron skin thickness ( $\Delta R_{\text{np}}$ ) in finite nuclei is crucial for constraining the density dependence of the nuclear symmetry energy. In this work, we systematically investigate  $\Delta R_{\text{np}}$  in the transuranium berkelium (Bk) isotopic chain using the deformed relativistic Hartree-Bogoliubov theory in continuum (DRHBc). Our results reveal a general increase of  $\Delta R_{\text{np}}$  with neutron number  $N$ , which exhibits anti-kinks at the shell closures  $N = 184, 258$  due to the shell effects. By decomposing  $\Delta R_{\text{np}}$  into volume and surface contributions through two-parameter Fermi (2pF) fits to angle-averaged DRHBc densities, we find that the volume term accounts for as much as 68% in most nuclei, whereas the surface term dominates only near the proton drip line for  $N < 142$ . Nuclear deformation is shown to slightly reduce the central radius  $R_c$  while significantly enhancing the surface diffuseness  $a$ , resulting in a notable increase in  $\Delta R_{\text{np}}$  that is largely driven by the surface term. Moreover, by extracting 2pF parameters along the symmetry axis ( $\theta = 0^\circ$ ) and perpendicular to it ( $\theta = 90^\circ$ ), we examine the anisotropy of  $\Delta R_{\text{np}}$ . In prolate deformed nuclei, a pronounced directional dependence emerges: although the nucleus elongates along the symmetry axis,  $\Delta R_{\text{np}}$  is substantially larger in the perpendicular direction. This anisotropy is weak for oblate nuclei near shell closures. The anisotropy of  $\Delta R_{\text{np}}$  is attributed mainly to the volume term, which remains the dominant contribution in most nuclei regardless of direction. These findings provide new insights into the interplay between deformation, shell structure, and the neutron skin in finite nuclei.

## I. INTRODUCTION

The neutron skin thickness, defined as the difference between the root-mean-square (rms) radii of the neutron and proton density distributions,  $\Delta R_{\text{np}} = r_n - r_p$ , plays an indispensable role in nuclear physics and astrophysics [1–4]. It is well established that  $\Delta R_{\text{np}}$  is strongly correlated with the density dependence of the nuclear symmetry energy  $E_{\text{sym}}(\rho)$  around the saturation density  $\rho_{\text{sat}}$  [5–9]. This correlation is commonly quantified by the slope parameter  $L = 3\rho_{\text{sat}} \partial E_{\text{sym}}(\rho)/\partial \rho|_{\rho_{\text{sat}}}$  [9–12], which characterizes the stiffness of the symmetry energy. For example, a strong linear correlation  $\Delta R_{\text{np}} = 0.101 + 0.00147L$  has been demonstrated for  $^{208}\text{Pb}$  [13]. A thicker neutron skin corresponds to a larger value of  $L$ , indicating higher pressure in neutron-rich matter. Therefore, an accurate determination of  $\Delta R_{\text{np}}$  in heavy nuclei provides crucial constraints on the density dependence of the nuclear symmetry energy, which has broad implications across multiple domains of physics, such as the structure and reactions of exotic nuclei, the location of nuclear drip lines, nuclear masses, density distributions, collective excitations, and the heavy-ion collision dynamics in nuclear physics [9, 11, 14–17], as well as neutron star structure, supernova explosions, neutrino emission, magnetar giant flares, and gravitational wave signals from neutron star mergers in astrophysics [18–22].

In laboratory, the radius of proton density distribution can be determined with high precision by electromagnetic

interactions. For instance, the charge radius of  $^{208}\text{Pb}$  has been accurately measured as  $r_{\text{ch}} = 5.5010(9)$  fm [23]. In contrast, directly and accurately measuring the neutron radius remains challenging. Indirect experimental approaches have been developed to probe the neutron distribution, including hadronic scattering [24, 25], studies of antiprotonic atoms [26], parity-violating electron scattering [27, 28], giant dipole resonance [29], and spin dipole resonances [30]. However, results from these methods often have large uncertainties and tend to be model-dependent. For example, analyses based on antiprotonic atom data [26] typically assume a specific nucleon density shape, such as a two-parameter Fermi distribution, introducing unavoidable systematic uncertainties into the extraction of  $\Delta R_{\text{np}}$ .

The formation of the neutron skin can arise from either an increase in the volume nuclear radius or an enhancement of the surface diffuseness. The relative significance of these volume and surface contributions is systematically influenced by the stiffness of the nuclear symmetry energy [31, 32]. Specifically, in the case of a soft symmetry energy ( $L \sim 20\text{--}60$  MeV), the neutron skin thickness of  $^{208}\text{Pb}$  comprises nearly equal parts from volume and surface effects; when the symmetry energy becomes very soft ( $L < 20$  MeV), the surface contribution becomes dominant, accounting for about 75% of the total thickness; and conversely, in cases with a stiff symmetry energy ( $L > 75$  MeV), approximately two-thirds of the neutron skin originates from the volume contribution [32]. This systematic relationship underscores the necessity of carefully considering the separation of volume and surface effects when describing neutron skin thickness, as well as incorporating observational constraints when extracting symmetry energy parameters from neutron star

---

\*Corresponding author, [ttsunphy@zzu.edu.cn](mailto:ttsunphy@zzu.edu.cn)

properties. Furthermore, the analysis of density distributions for  $^{208}\text{Pb}$  in PREX II experiment reveals a pronounced excess of neutrons over protons both in the inner core and the surface region, highlighting the importance of both volume and surface distributions to the symmetry energy in finite nuclei [33].

In this study, we investigate the neutron skin thickness and the associated volume and surface contributions in transuranium berkelium (Bk) isotopes. As established in our previous work [34], most Bk isotopes are deformed, which significantly reshapes the proton and neutron density distributions and enlarges the nuclear rms radii significantly. Moreover, deformation may modify the neutron skin thickness and could even induce an anisotropy in the neutron skin. Motivated by these deformation correlations, the present study, like our earlier investigation [34], adopts the deformed relativistic Hartree-Bogoliubov theory in continuum (DRHBc) [35–40], which provides a unified description of nuclear deformation, pairing correlations, and continuum effects. Until now, DRHBc theory has achieved remarkable successes in nuclear study, such as the establishment of nuclear mass table [38–42]; the investigation of shell structure and the prediction of nuclear magic numbers [34, 43–46]; the exploration of the neutron drip line [47] and novel physical phenomena such as the possible existence of bound nuclei beyond it [48–50] and odd-even differences in the stability “peninsula” [51]; the studies on pairing energy [52], one-proton emission [53], and  $\alpha$ -decay half lives [54, 55]; the description of nuclear charge radii [56–59]; and the extensive research on nuclear shapes, covering shape evolution [34, 57, 60], shape coexistence [34, 56, 61, 62], prolate dominance [63], bubble structures [64], and inner fission barriers [65]. Furthermore, the theory has advanced the investigation of halo phenomena, including giant halos [66], deformed two-neutron halos [67], and nuclear magnetism in the deformed halo nuclei [68], while its extensions have enabled studies of shape decoupling effects and rotation of deformed halos [69, 70], halos in triaxial nuclei [71], and unified descriptions of halo nuclei from microscopic structure to reaction observables [72, 73]. The reliability of the DRHBc theory is well demonstrated by its predictive performance. Within the DRHBc mass table based on the PC-PK1 functional [74], systematic calculations for even- $Z$  nuclei with  $8 \leq Z \leq 120$  reproduce the available data with a rms deviation of  $\sigma = 1.433$  MeV for binding energies [50, 75, 76], and  $\sigma = 0.033$  fm for charge radii [41], highlighting its great advantage in predicting masses and radii. Recent examinations of the superheavy nuclear masses and newly measured mass data further underscore the precision of DRHBc mass descriptions [50, 51, 77]. Besides, the DRHBc calculation for  $^{208}\text{Pb}$  [56] gives a neutron skin thickness of  $\Delta R_{\text{np}} = 0.257$  fm, consistent with the PREX-II experimental result of  $0.283 \pm 0.071$  fm within uncertainties [33].

The present study aims to achieve two main objectives. First, we examine the relative contributions of the

volume and surface terms to  $\Delta R_{\text{np}}$  and their evolution along the Bk isotopic chain. Second, we explore the possible anisotropy of the neutron skin by comparing its values along and perpendicular to the symmetry axis. To quantify the neutron skin thickness, we fit the DRHBc density profiles with a two-parameter Fermi (2pF) distribution using the Levenberg-Marquardt algorithm [31], from which the neutron skin thickness as well as its volume and surface contributions are derived. For comparison, we also present results obtained by fitting densities from spherical relativistic continuum Hartree-Bogoliubov (RCHB) calculations [78], allowing us to assess the influence of deformation.

The paper is organized as follows. Section II briefly introduces the DRHBc theory and the formalism for neutron skin thickness along with the volume and surface contributions. After the numerical details in Sec. III, results and discussions are presented in Sec. IV. Finally, a summary is given in Sec. V.

## II. THEORETICAL FRAMEWORK

### A. DRHBc theory

Detailed descriptions of the DRHBc theory can be found in Refs. [35–38]. Here, for the convenience in discussions, we briefly introduce the formalism. In the DRHBc theory, the relativistic Hartree-Bogoliubov (RHB) equation reads,

$$\begin{pmatrix} \hat{h}_D - \lambda & \hat{\Delta} \\ -\hat{\Delta}^* & -\hat{h}_D^* + \lambda \end{pmatrix} \begin{pmatrix} U_k \\ V_k \end{pmatrix} = E_k \begin{pmatrix} U_k \\ V_k \end{pmatrix}, \quad (1)$$

where  $\hat{h}_D$  represents the Dirac Hamiltonian,  $\hat{\Delta}$  is the pairing potential,  $\lambda$  is the Fermi energy for neutrons or protons,  $E_k$  is the quasiparticle energy, and  $U_k$  and  $V_k$  are the quasiparticle wave functions.

The Dirac Hamiltonian in the coordinate space is given by

$$h_D(\mathbf{r}) = \boldsymbol{\alpha} \cdot \mathbf{p} + V(\mathbf{r}) + \beta[M + S(\mathbf{r})], \quad (2)$$

where  $M$  is the nucleon mass, and  $S(\mathbf{r})$  and  $V(\mathbf{r})$  are the scalar and vector potentials, respectively. The pairing potential is expressed as,

$$\Delta(\mathbf{r}_1, \mathbf{r}_2) = V^{pp}(\mathbf{r}_1, \mathbf{r}_2) \kappa(\mathbf{r}_1, \mathbf{r}_2), \quad (3)$$

where  $\kappa = V^*U^T$  is the pairing tensor and  $V^{pp}$  is the pairing force in a density-dependent zero-range type,

$$V^{pp}(\mathbf{r}_1, \mathbf{r}_2) = V_0 \frac{1}{2} (1 - P^\sigma) \delta(\mathbf{r}_1 - \mathbf{r}_2) \left( 1 - \frac{\rho(\mathbf{r}_1)}{\rho_{\text{sat}}} \right), \quad (4)$$

with  $V_0$  being the pairing strength,  $\frac{1}{2}(1 - P^\sigma)$  the projector for the spin  $S = 0$  component, and  $\rho_{\text{sat}}$  the saturation density of nuclear matter.

For an axially deformed nucleus with spatial reflection symmetry, the third component  $\Omega$  of the angular momentum  $j$  and the parity  $\pi$  are conserved quantum numbers. Thus, the RHB Hamiltonian can be decomposed into blocks  $\Omega^\pi$  characterized by  $\Omega$  and parity  $\pi$ . Additionally, the potentials and densities in the DRHBc theory can be expanded in terms of Legendre polynomials [79],

$$f(\mathbf{r}) = \sum_{\lambda} f_{\lambda}(r) P_{\lambda}(\cos \theta), \quad \lambda = 0, 2, 4, \dots, \quad (5)$$

with

$$f_{\lambda}(r) = \frac{2\lambda + 1}{4\pi} \int d\Omega f(\mathbf{r}) P_{\lambda}(\cos \theta). \quad (6)$$

The diagonalization of the RHB matrix gives the quasiparticle wave functions, which can be employed to construct densities and potentials.

The rms radius is defined as

$$r_{\tau} = \langle r^2 \rangle^{1/2} = \sqrt{\frac{\int d^3\mathbf{r} [r^2 \rho_{\tau}(\mathbf{r})]}{N_{\tau}}}, \quad (7)$$

where  $\rho_{\tau}(\mathbf{r})$  is the vector density,  $N_{\tau}$  denotes the particle number, and the subscript  $\tau$  refers to neutron, proton, or nucleon.

The quadrupole deformation is calculated by

$$\beta_{\tau,2} = \frac{\sqrt{5\pi} Q_{\tau,2}}{3N_{\tau} \langle r_{\tau}^2 \rangle}, \quad (8)$$

where  $Q_{\tau,2}$  is the intrinsic quadrupole moment,

$$Q_{\tau,2} = \sqrt{\frac{16\pi}{5}} \langle r^2 Y_{20}(\theta, \phi) \rangle. \quad (9)$$

For an odd- $A$  or odd-odd nucleus, the blocking effect of the unpaired nucleon is treated within the DRHBc theory using the equal filling approximation [37, 39].

### B. Neutron skin thickness: volume and surface contributions

To decompose the neutron skin thickness into surface and volume contributions, we adopt the widely used 2pF distribution for the nuclear density,

$$\rho(r) = \frac{\rho_0}{1 + \exp[(r - C)/a]}, \quad (10)$$

where the diffuseness parameter  $a$  and the half-density radius  $C$  are obtained by fitting the densities from DRHBc calculations using the Levenberg-Marquardt algorithm, while the central density  $\rho_0 \approx \rho(0)$  is fixed by the constraint of proton or neutron number,

$$\int \rho(r) d^3\mathbf{r} = 4\pi \int_0^{\infty} \rho(r) r^2 dr = Z \text{ or } N. \quad (11)$$

Several definitions are commonly employed to characterize nuclear size. As systematically detailed by Hasse and Myers [80], the most intuitive descriptor is the central radius  $C$ , which coincides with the radius at half-density for the 2pF distribution.

The equivalent sharp radius  $R$  is defined as the radius of a sharp distribution with a uniform density corresponding to the nuclear central value  $\rho(0)$ ,

$$\frac{4}{3}\pi R^3 \rho(0) = 4\pi \int_0^{\infty} \rho(r) r^2 dr. \quad (12)$$

Another equivalent radius is the quadratic radius  $Q$ , which can be derived directly from electron scattering experiments [81] and defined by

$$\frac{3}{5}Q^2 = \langle r^2 \rangle. \quad (13)$$

The surface width  $b$  quantifies the diffuseness of the nuclear surface. It is derived from the normalized surface weight function

$$g(r) = -\frac{1}{\rho(0)} \frac{d\rho(r)}{dr}, \quad (14)$$

which is positive for a monotonically decreasing density. The width  $b$  is given by the square root of the second central moment of  $g(r)$ ,

$$b^2 = \int_0^{\infty} (r - C)^2 g(r) dr, \quad (15)$$

providing a globally averaged measure of the surface thickness.

For a 2pF distribution,  $b$  relates simply to the diffuseness  $a$  via

$$b = \frac{\pi}{\sqrt{3}} a. \quad (16)$$

Similarly, the surface thickness  $t$ , defined as the distance over which the density drops from 90% to 10% of central density  $\rho(0)$ , is linked to  $b$  by

$$t = \frac{4\sqrt{3} \log 3}{\pi} b \approx 2.42 b, \quad (17)$$

a relation specific to Fermi-type distributions [81].

Based on the surface expansion formalism introduced in Refs. [80, 81], radii  $C$  and  $Q$  can be approximately expressed by expansions in terms of  $R$  and the dimensionless ratio  $\xi = b/R$ , up to the first order in  $\xi^2$ ,

$$C \simeq R(1 - \xi^2), \quad (18)$$

$$Q \simeq R \left( 1 + \frac{5}{2} \xi^2 \right). \quad (19)$$

For thin-skinned nuclei ( $\xi \ll 1$ ), these approximations remain accurate.

The neutron skin thickness, quantifying the extra radial extent of neutrons relative to protons, is defined as

$$\Delta R_{\text{np}} = \langle r_{\text{n}}^2 \rangle^{1/2} - \langle r_{\text{p}}^2 \rangle^{1/2}. \quad (20)$$

Combining Eqs. (13), (19) and (20) yields a refined expression [31],

$$\Delta R_{\text{np}} = \sqrt{\frac{3}{5}} \left[ (R_{\text{n}} - R_{\text{p}}) + \frac{5}{2} \left( \frac{b_{\text{n}}^2}{R_{\text{n}}} - \frac{b_{\text{p}}^2}{R_{\text{p}}} \right) \right], \quad (21)$$

which separates the skin into two physically distinct contributions:

$$\Delta R_{\text{np}} = \Delta R_{\text{np}}^{\text{vol}} + \Delta R_{\text{np}}^{\text{surf}}, \quad (22)$$

with the volume part

$$\Delta R_{\text{np}}^{\text{vol}} \equiv \sqrt{\frac{3}{5}} (R_{\text{n}} - R_{\text{p}}), \quad (23)$$

and the surface part

$$\Delta R_{\text{np}}^{\text{surf}} \equiv \sqrt{\frac{3}{5}} \frac{5}{2} \left( \frac{b_{\text{n}}^2}{R_{\text{n}}} - \frac{b_{\text{p}}^2}{R_{\text{p}}} \right). \quad (24)$$

Thus, a neutron skin can form either through a difference in volume radii  $R$  between neutrons and protons, or through differences in the surface diffuseness width  $b$ , or a combination of both.

We can also rewrite the volume and surface contributions to the neutron skin thickness in Eqs. (23-24) directly in terms of the 2pF parameters in Eq. (10) using Eq. (16) and the expansion (18) as the following,

$$\Delta R_{\text{np}}^{\text{vol}} = \sqrt{\frac{3}{5}} \left[ (C_{\text{n}} - C_{\text{p}}) + \frac{\pi^2}{3} \left( \frac{a_{\text{n}}^2}{C_{\text{n}}} - \frac{a_{\text{p}}^2}{C_{\text{p}}} \right) \right], \quad (25)$$

and

$$\Delta R_{\text{np}}^{\text{surf}} = \sqrt{\frac{3}{5}} \frac{5\pi^2}{6} \left( \frac{a_{\text{n}}^2}{C_{\text{n}}} - \frac{a_{\text{p}}^2}{C_{\text{p}}} \right). \quad (26)$$

For a deformed nucleus, the 2pF parameters in Eq. (10) are determined by fitting the DRHBc density averaged over angles or along the symmetry axis ( $\theta = 0^\circ$ ) and perpendicular to it ( $\theta = 90^\circ$ ).

### III. NUMERICAL DETAILS

All numerical details adopted in this work follow those used in the construction of the DRHBc mass tables [38–41]. To treat the continuum effects properly, the DRHB equations are solved in the Dirac Woods-Saxon (DWS) basis [82, 83]. The following numerical cutoffs and parameters are employed: the angular momentum cutoff in the DWS basis is set to  $J_{\text{max}} = \frac{23}{2}h$ ; the maximum order of expansion in Eq. (5) is  $\lambda_{\text{max}} = 8$ , which has

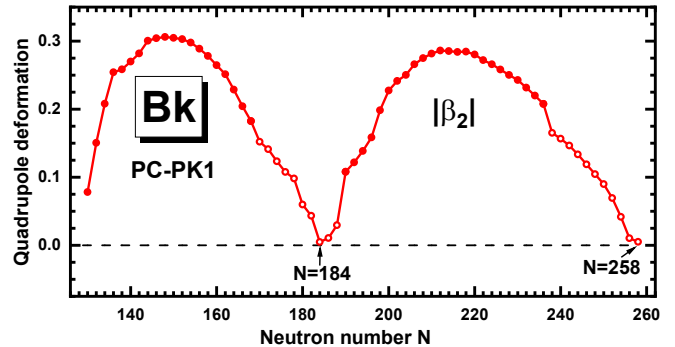


Figure 1: (Color online) Evolution of the quadrupole deformation  $|\beta_2|$  for the Bk isotopes in ground states as a function of the neutron number  $N$  obtained by the DRHBc calculations with PC-PK1 density functional. The solid circles denote prolate shapes with positive  $\beta_2$  while the open circles denote oblate shapes with negative  $\beta_2$ .

been shown sufficient in previous studies [39, 84]; the box size is set to 20 fm; and the energy cutoff in the Fermi sea is  $E_{\text{cut}}^+ = 300$  MeV. For particle-hole channel, the PC-PK1 [74] density functional is taken. For the particle-particle channel, a zero-range pairing force is used with a saturation density  $\rho_{\text{sat}} = 0.152 \text{ fm}^{-3}$  and a pairing strength  $V_0 = -325 \text{ MeV}\cdot\text{fm}^3$  [40].

## IV. RESULTS AND DISCUSSION

This work systematically investigates the neutron skin thickness in odd- $A$  transuranium Bk isotopes, along with its decomposition into volume and surface contributions. First, in Subsec. IV A, we present the neutron skin thickness obtained directly from self-consistent DRHBc and spherical RCHB calculations. Then, in Subsec. IV B, the neutron skin thickness is decomposed into volume and surface terms using 2pF parameters fitted to the angle-averaged DRHBc densities; the influence of deformation is quantified by comparison with spherical RCHB results. Finally, in Subsec. IV C, we examine the anisotropy of the neutron skin thickness along different orientations relative to the symmetry axis.

### A. Neutron skin thickness of Bk isotopes

In Fig. 1, for the convenience of discussion, we plot the evolution of the quadrupole deformation  $|\beta_2|$  for Bk isotopes in the ground states from the proton drip line to the neutron drip line, which are calculated by DRHBc theory with the PC-PK1 density functional. Open and solid circles denote shapes in oblate ( $\beta_2 < 0$ ) and prolate ( $\beta_2 > 0$ ), respectively. Obvious shell structures can be observed with vanishing deformation at neutron closures of  $N = 184, 258$  while pronounced deformations around the mid-shells. Besides, prolate dominance can be found

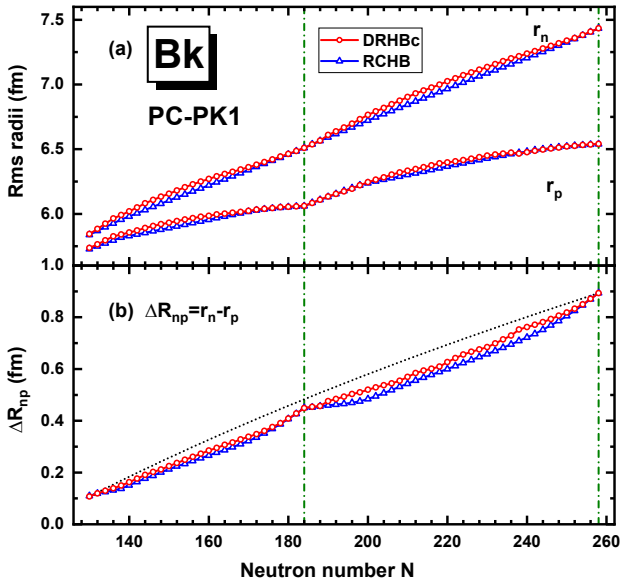


Figure 2: (Color online) (a) Rms radius for neutrons ( $r_n$ ) and protons ( $r_p$ ), and (b) neutron skin thickness  $\Delta R_{np}$ , as functions of the neutron number  $N$  in Bk isotopes, obtained by the self-consistent DRHBc calculations. Spherical RCHB results [78] are included for comparison. The dashed line in panel (b) linking the values of the proton and neutron drip-line nuclei is given to guide the eye.

along the whole isotopic chain [34].

Figure 2 presents the rms radii for neutrons  $r_n$  and protons  $r_p$ , together with the neutron skin thickness  $\Delta R_{np} = r_n - r_p$ , for Bk isotopes as functions of neutron number  $N$ , obtained from DRHBc calculations with the PC-PK1 density functional. Both  $r_n$  and  $r_p$  generally increase with  $N$ , showing noticeable kinks at the neutron magic numbers  $N = 184$  and  $N = 258$ . In particular, the growth rates of neutron and proton rms radii differ significantly across the shell closure at  $N = 184$ : the neutron radius increases steadily both before and after the closure, whereas the proton radius rises slowly before the closure but more rapidly afterward, a behavior driven by the  $np$  interaction between valence neutrons and protons. Consequently, this shell-induced difference in the growth rates leads directly to a pronounced anti-kink in  $\Delta R_{np}$  around the neutron shell closures, even though it follows an overall increasing trend with  $N$ . Besides, when comparing DRHBc calculations with the spherical RCHB results [78], obvious deformation effect has been suggested to extend the nuclear spatial distributions as well as the neutron skin thickness.

### B. Neutron skin thickness averaged over angles: volume and surface contributions

To figure out the volume and surface contributions to neutron skin thickness, it turns out that the definition of the nuclear radius must be chosen properly. In Fig. 3,

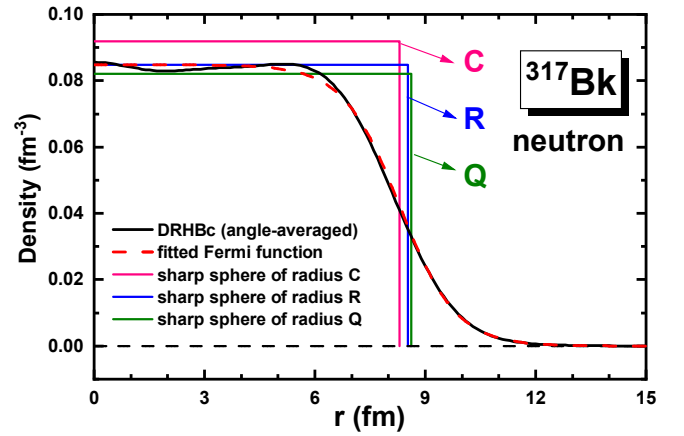


Figure 3: (Color online) Neutron density distribution in  $^{317}\text{Bk}$ . The black solid line denotes the angle-averaged DRHBc result, while the red dashed line represents the corresponding 2pF fit. For comparison, sharp surface density profiles characterized by the central radius  $C$ , the equivalent sharp radius  $R$ , and the equivalent rms radius  $Q$  are also included.

taking the deformed nucleus  $^{317}\text{Bk}$  as an example, the neutron density distribution obtained by DRHBc calculation and the corresponding 2pF fitted profile are displayed. Also shown are sharp-surface densities defined via the central radius  $C$ , the equivalent sharp radius  $R$ , and the quadratic radius  $Q$ . The fitting was performed using the Levenberg–Marquardt algorithm for nonlinear least-squares minimization with the central density constrained by the neutron number. As seen in Fig. 3, the sharp surface density profile with central radius  $C$  overestimates the volume density, while that based on quadratic radius  $Q$  underestimates it. It is only the profile defined using the equivalent sharp radius  $R$  that can reproduce the volume density properly. Therefore,  $R$  is adopted in the following for calculating the neutron skin thickness as well as the volume and surface contributions by Eqs. (22-24).

In Fig. 4, we present the 2pF parameters for neutrons and protons in the Bk isotopic chain including the half-density radius  $R_c$  ( $\equiv C$ ), diffusion coefficient  $a$ , and central density  $\rho_0$ , fitted by the DRHBc density distributions averaged over angles (panels a-c) using the PC-PK1 density functional. For comparison, the 2pF parameters from spherical RCHB densities (panels d-f) are also given. Solid symbols denote nuclei at the  $N = 184$  shell closure, and dashed lines indicate the corresponding reference values of  $R_c$ ,  $a$ , and  $\rho_0$ . All 2pF parameters fitted by DRHBc and RCHB densities are consistent well with each other at  $N = 184$  for both neutrons and protons.

In panels (a) and (d), the half-density radii  $R_c$  obtained by fitting DRHBc and RCHB densities exhibit similar trend in Bk isotopes: a general increase with neutron number  $N$  with some localized deviations around the magic number  $N = 184$ , which correspond to the kinks observed in the neutron and proton rms radii in

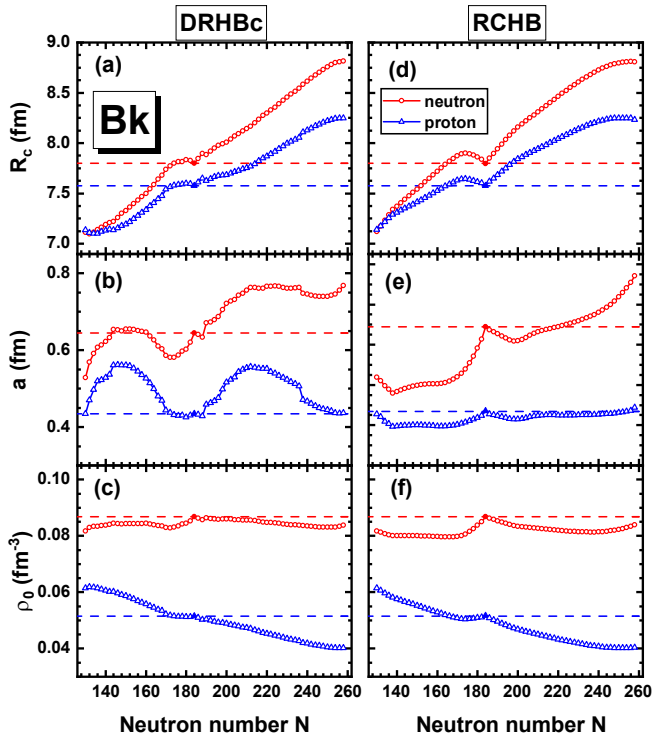


Figure 4: (Color online) Proton and neutron 2pF parameters in Eq. (10), radius  $R_c$ , diffuseness  $a$ , and central density  $\rho_0$ , obtained by fitting the density distributions from (a-c) angle-averaged DRHBc and (d-f) RCHB calculations under charge number constraints. Solid symbols mark the nucleus at the shell closure  $N = 184$ , and dashed lines indicate its parameter values.

Fig. 2(a). In panels (b) and (e), the evolution of the diffusion coefficients  $a$  shows obvious different behaviors between the two theories: the spherical RCHB results show an increasing diffusion coefficient  $a$  for neutrons and almost constant  $a$  for protons, both marked by anti-kinks at the shell closure  $N = 184$ ; in the DRHBc case, deformation becomes the key factor, due to which the proton  $a_p$  closely follows the deformation trend in Fig. 1 and neutron  $a_n$  is governed by the combined effects of increasing neutron number, shell structure, and deformation. In panels (c) and (f), the central density  $\rho_0$  determined by particle number constraints, behaves similarly in both theories: the neutron central density remains nearly constant, while the proton central density gradually decreases due to the increasing proton radius  $R_c$  in panels (a) and (d).

To further examine the influence of deformation on the 2pF parameters  $R_c$ ,  $a$ , and  $\rho_0$ , Fig. 5 shows the ratios between the values obtained from DRHBc and those from spherical RCHB calculations. Circles and triangles represent results for neutrons and protons, respectively. Compared with the quadrupole deformation evolution in Fig. 1, panel (a) reveals that the ratio  $R_c^{\text{DRHBc}}/R_c^{\text{RCHB}}$  deviates only slightly from one, even for large deformations. This indicates that quadrupole deformation, no

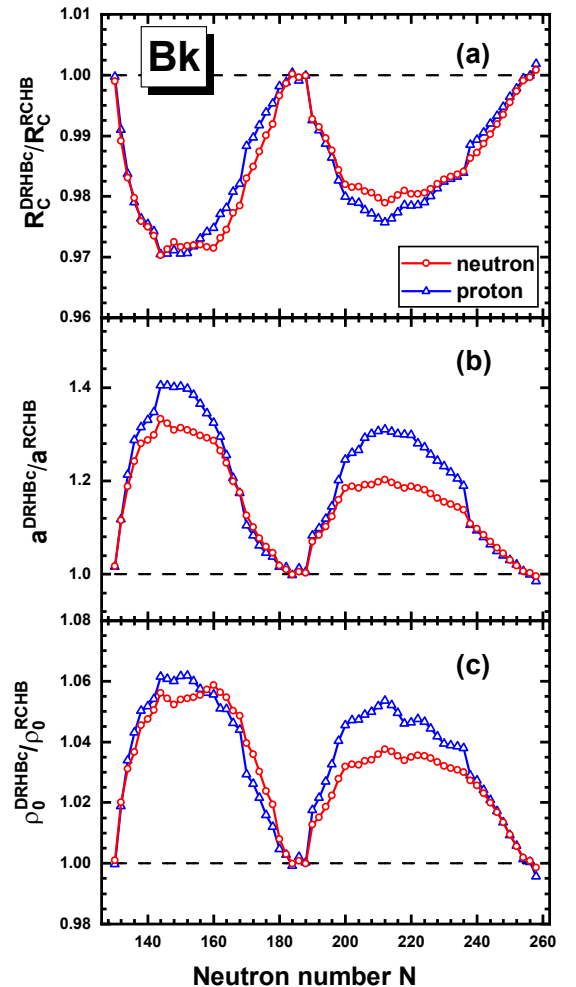


Figure 5: (Color online) Ratios of DRHBc to RCHB results for the (a) radius  $R_c$ , (b) diffuseness  $a$ , and (c) central density  $\rho_0$ . Circles and triangles represent results for neutrons and protons, respectively.

matter prolate or oblate shape, tends to contract the central radius  $R_c$  slightly, an effect opposite to the great expansion seen in the rms radii in Fig. 2. In contrast, panel (b) shows that the diffuseness ratio  $a^{\text{DRHBc}}/a^{\text{RCHB}}$  increases markedly with deformation, reaching enhancements of up to 40% relative to the spherical case. This demonstrates that deformation significantly enlarges the surface diffuseness for both prolate and oblate nuclei. Panel (c) indicates that deformation also raises the central density  $\rho_0$  modestly compared to the spherical case. This reflects a radial compression effect in which deformation drives nuclear matter toward the center, thereby increasing the central density. In summary, deformation slightly reduces the central radius  $R_c$  and increases the central density  $\rho_0$ , while significantly enhancing the diffusion coefficient  $a$ .

In Fig. 6, we present neutron skin thickness  $\Delta R_{\text{np}}$  along with the volume  $\Delta R_{\text{np}}^{\text{vol}}$  and surface  $\Delta R_{\text{np}}^{\text{surf}}$  components as functions of the neutron number  $N$  in Bk

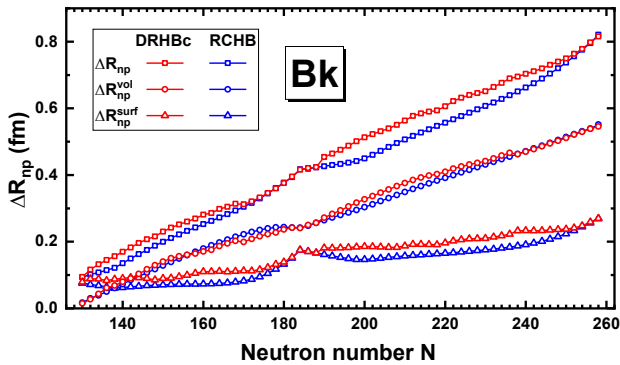


Figure 6: (Color online) Neutron skin thickness  $\Delta R_{np}$ , along with its volume ( $\Delta R_{np}^{\text{vol}}$ ) and surface ( $\Delta R_{np}^{\text{surf}}$ ) components, as functions of neutron number  $N$  in Bk isotopes. The values are calculated using Eqs. (22-24) with the 2pF parameters in Fig. 4, obtained by fitting the angle-averaged DRHBc and RCHB densities.

isotopes, with the 2pF parameters shown in Fig. 4 determined by fitting the DRHBc and RCHB densities. For spherical nuclei around the magic closures  $N = 184$  and  $N = 258$ , the neutron skin thicknesses  $\Delta R_{np}$  predicted by DRHBc and RCHB are nearly identical. For the other nuclei which are deformed, the neutron skin thickness by DRHBc is larger than those obtained by spherical RCHB. Besides, larger absolute deformation magnitudes lead to more pronounced enhancements in the neutron skin thickness, indicating that nuclear deformation plays a vital role in determining  $\Delta R_{np}$ . When separating the neutron skin thickness into volume and surface contributions, both DRHBc and RCHB predictions show that the volume term  $\Delta R_{np}^{\text{vol}}$  dominates  $\Delta R_{np}$  for most nuclei and the contribution can reach to 68% in the neutron-rich side while the surface contribution  $\Delta R_{np}^{\text{surf}}$  surpasses the volume component  $\Delta R_{np}^{\text{vol}}$  only when  $N < 142$  around the proton drip line. A further comparison between the DRHBc and RCHB results reveals notable discrepancies in the surface term  $\Delta R_{np}^{\text{surf}}$  but only minor ones in the volume term  $\Delta R_{np}^{\text{vol}}$ . This indicates that the deformation-induced enhancement in neutron skin thickness originates primarily from the surface contribution. This can be explained by the great increase of the diffusion coefficient  $a$  due to the deformation as shown in Fig. 5(b) while slight reduction for the central radii  $R_c$  as shown in Fig. 5(a).

### C. Neutron skin thickness along $\theta = 0^\circ, 90^\circ$ : volume and surface contributions

In this section, we further investigate the anisotropy of the neutron skin thickness  $\Delta R_{np}$  with respect to spatial direction. For this purpose, the 2pF parameters ( $R_c$ ,  $a$ , and  $\rho_0$ ) are extracted from DRHBc density distributions along the symmetry axis ( $z, \theta = 0^\circ$ ) and perpendicular to it ( $r_\perp = \sqrt{x^2 + y^2}, \theta = 90^\circ$ ), respectively. Figure 7 displays the density distributions along  $\theta = 0^\circ$  (a,

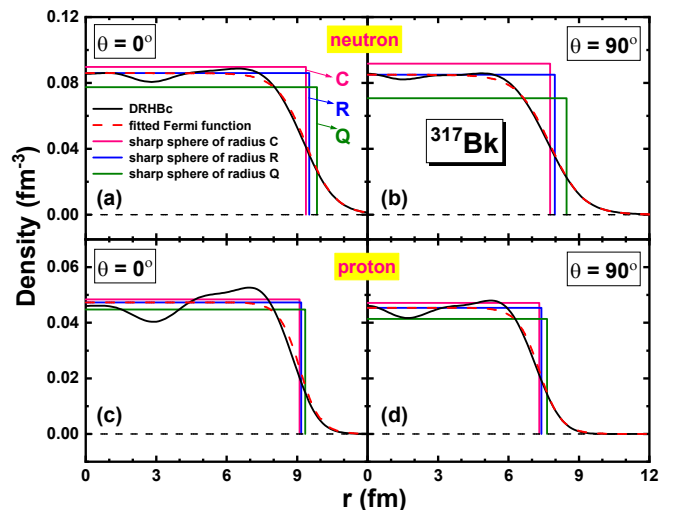


Figure 7: (Color online) Same as Fig. 3, but showing fits to the DRHBc density distributions along the symmetry axis ( $z, \theta = 0^\circ$ ) in (a, c) and perpendicular to that axis ( $r_\perp = \sqrt{x^2 + y^2}, \theta = 90^\circ$ ) in (b, d), for neutrons (a, b) and protons (c, d).

c) and  $\theta = 90^\circ$  (b, d) for neutrons (a, b) and protons (c, d) in  $^{317}\text{Bk}$ . The black solid curves represent the DRHBc results, while the red dashed curves correspond to the 2pF fits obtained via the Levenberg-Marquardt algorithm. For comparison, sharp surface density profiles characterized by the central radius  $C$ , the equivalent sharp radius  $R$ , and the quadratic radius  $Q$  are also included. In all panels, the equivalent sharp radius  $R$  matches the volume density properly compared with  $C$  and  $Q$ . Therefore,  $R$  is used to calculate the neutron skin thickness via Eqs. (22-24).

Figure 8 shows the 2pF parameters ( $R_c$ ,  $a$ ,  $\rho_0$ ) extracted from fitting the DRHBc density along the symmetry axis ( $\theta = 0^\circ$ ) and perpendicular to it ( $\theta = 90^\circ$ ), plotted as functions of neutron number  $N$  in Bk isotopic chain. As shown in panels (a) and (d), the central radius  $R_c$  exhibits strong directional dependence. For prolate nuclei in mass regions  $130 \leq N \leq 168$  and  $190 \leq N \leq 236$ , as they are elongated along the symmetry axis  $z$ ,  $R_c$  is significantly larger along  $\theta = 0^\circ$  than along  $\theta = 90^\circ$ . In contrast, for oblate nuclei in the mass range of  $170 \leq N \leq 182$  and  $238 \leq N \leq 256$ , as they are flattened perpendicular to the symmetry axis,  $R_c$  is larger along  $\theta = 90^\circ$  than along  $\theta = 0^\circ$ . In panels (b) and (e), the diffuseness parameter  $a$  exhibits opposite dependence on spatial direction to those for central radius  $R_c$ , i.e., prolate deformation will increase the diffuseness  $a$  along  $\theta = 90^\circ$  while oblate deformation increases  $a$  along  $\theta = 0^\circ$  both for neutrons and protons. In panels (c) and (f), the central densities  $\rho_0$ , which are determined by particle number constraints along the symmetry axis  $z$  and the perpendicular direction respectively, exhibits no pronounced dependence on spatial direction both for neutrons and protons. Besides, with increasing neutron

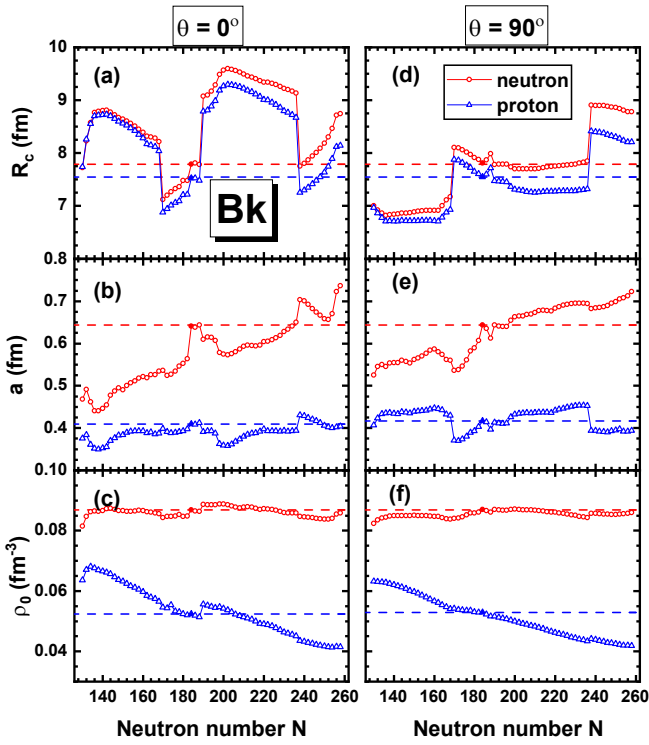


Figure 8: (Color online) Same as Fig. 4, but here fitted to the DRHBc density distributions along the symmetry axis ( $z$ ,  $\theta = 0^\circ$ ) in panels (a-c), and perpendicular to the symmetry axis ( $r_\perp$ ,  $\theta = 90^\circ$ ) in panels (d-f).

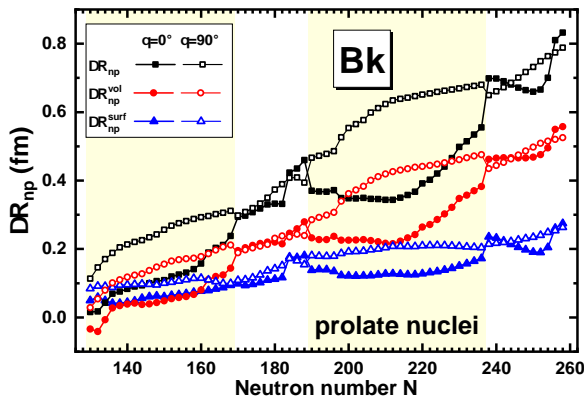


Figure 9: (Color online) Same as Fig. 6, but showing the neutron skin thickness  $\Delta R_{np}$  along with its volume ( $\Delta R_{np}^{\text{vol}}$ ) and surface ( $\Delta R_{np}^{\text{surf}}$ ) components along the symmetry axis ( $z$ ,  $\theta = 0^\circ$ ) and perpendicular to that axis ( $r_\perp$ ,  $\theta = 90^\circ$ ). The yellow region represents nuclei with a prolate deformation.

number  $N$ , the neutron central density remains approximately constant, whereas the proton central density exhibits an overall decreasing trend.

In Fig. 9, we present the neutron skin thickness  $\Delta R_{np}$  as well as the volume and surface contributions both

along the symmetry axis ( $\theta = 0^\circ$ ) and perpendicular to the symmetry axis ( $\theta = 90^\circ$ ) to study the anisotropy. The 2pF parameters shown in Fig. 8 are adopted to do the calculations. A strong directional dependence is observed for neutron skin thickness in prolate deformed nuclei, although they are elongated along the symmetry axis  $z$ , the  $\Delta R_{np}$  perpendicular to the symmetry axis ( $\theta = 90^\circ$ ) is significantly larger than that along the symmetry axis  $\theta = 0^\circ$ . In contrast, for nuclei in oblate shapes near the magic closures  $N = 184, 258$ , this anisotropy is reduced and the values of  $\Delta R_{np}$  along  $\theta = 0^\circ$  and  $\theta = 90^\circ$  are very close. It is noted that a tiny anisotropy in the neutron skin thickness is still observed for the magic nuclei with  $N = 184$  and  $N = 258$ , due to their slight nuclear deformation: the quadrupole deformations for neutrons, protons, and the total system are  $\beta_2 = -0.003, -0.007, -0.005$  and  $\beta_2 = -0.003, -0.010, -0.005$ , respectively. When decomposing the  $\Delta R_{np}$  into the volume and surface terms, similar anisotropy has been shown in the prolate nuclei. For the volume term  $\Delta R_{np}^{\text{vol}}$  which are related with  $R_n - R_p$ , although the central radii  $R_{n,p}$  are larger along  $\theta = 0^\circ$  both for neutrons and protons,  $\Delta R_{np}^{\text{vol}}$  is smaller along  $\theta = 0^\circ$ . For the surface term  $\Delta R_{np}^{\text{surf}}$  which is related with  $b_n^2/R_n - b_p^2/R_p$ , as the diffuseness  $a$  along  $\theta = 90^\circ$  is larger than that along  $\theta = 0^\circ$  in prolate nuclei,  $\Delta R_{np}^{\text{surf}}$  remains larger along  $\theta = 90^\circ$ . When comparing the contributions from the volume and surface terms, it's found that the volume term dominates  $\Delta R_{np}$  as much as 65% in most nuclei with some exceptions near the proton drip line. It is observed that along the symmetry axis  $\theta = 0^\circ$ , the surface contribution is dominant for nuclei only with  $N < 160$ , and along the direction  $\theta = 90^\circ$ , the surface contribution is dominant in fewer nuclei only with  $N < 136$ . Especially, it's noted that the volume contributions in nuclei with  $N = 130, 132, 134$  are negative along  $\theta = 0^\circ$  as a consequence of  $R_p > R_n$  slightly in those nuclei as shown in Fig. 8(a).

Finally, taking the prolate deformed nucleus  $^{317}\text{Bk}$  as an example, Fig. 10 displays the two-dimensional density distribution  $\rho(r)/\rho_0$  for protons (left panel) and neutrons (right panel). The color scale indicates the density relative to the central density  $\rho_0$ , ranging from 0% to 100%. To intuitively access the surface and volume contributions to the neutron skin thickness, we provide the surface thickness  $t$ , defined as the distance over which the density decreases from 90% to 10% of  $\rho_0$ , and the radii at half-density  $C$  for neutrons and protons, evaluated both along the symmetry axis ( $z$ ,  $\theta = 0^\circ$ ) and perpendicular to it ( $x$ ,  $\theta = 90^\circ$ ).

For this prolate nucleus, the density distributions of both neutrons and protons extend further along the symmetry axis ( $\theta = 0^\circ$ ) than in the perpendicular direction ( $\theta = 90^\circ$ ). The radii at half-density along the symmetry axis are  $C_n = 9.38$  fm and  $C_p = 9.10$  fm, significantly larger than those in the perpendicular direction ( $C_n = 7.77$  fm and  $C_p = 7.31$  fm). Those values are very close to the corresponding equivalent sharp



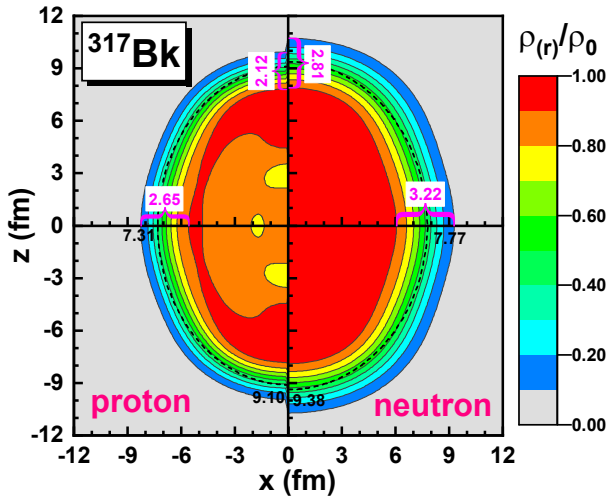


Figure 10: (Color online) Two-dimensional density distributions  $\rho(r)/\rho_0$  for neutrons (left) and protons (right) in  $^{317}\text{Bk}$ , plotted in the  $x$ - $z$  plane. The color scale indicates the density relative to the central density  $\rho_0$ , ranging from 0% to 100%. The surface thickness  $t$  (distance for the density to drop from 90% to 10% of  $\rho_0$ ) is given for each species along and perpendicular to the symmetry axis  $z$ . It relates to the surface term of neutron-skin thickness  $\Delta R_{\text{np}}^{\text{surf}}$  in Eq. (24) via  $t \approx 2.42b$ . Besides, the radii  $C_n$  and  $C_p$  at half-density are indicated by dash-dotted lines. These are close to the equivalent sharp radii  $R_n$  and  $R_p$ , which are associated with the volume term of neutron-skin thickness  $\Delta R_{\text{np}}^{\text{vol}}$  defined in Eq. (23).

radii:  $R_n = 9.51$  fm,  $R_p = 9.17$  fm along  $\theta = 0^\circ$  and  $R_n = 7.98$  fm,  $R_p = 7.41$  fm along  $\theta = 90^\circ$ . By comparing  $R_n$  and  $R_p$  along different directions, we find  $R_n - R_p = 0.34$  fm along the symmetry axis, which is smaller than the value of 0.57 fm in the perpendicular direction. This indicates a larger contribution from the volume term  $\Delta R_{\text{np}}^{\text{vol}}$  along  $\theta = 90^\circ$ . To analyse the surface contribution  $\Delta R_{\text{np}}^{\text{surf}}$ , we measure the surface thickness  $t$ , which is related to the diffuseness parameter  $b$  via  $t \approx 2.42b$ . The relative magnitudes of the diffuseness parameter  $t$  in different directions are opposite to those of the equivalent sharp radius  $R$ . Along the  $z$ -axis, we obtain  $t = 2.81$  fm for neutrons and 2.12 fm for protons, which are smaller than the values in the perpendicular direction with  $t = 3.22$  fm for neutrons and 2.65 fm for protons. According to Eq. (24), as the  $\Delta R_{\text{np}}^{\text{surf}}$  depends on the difference in  $b^2/R$  between neutrons and protons, the smaller diffuseness ( $t$  or  $b$ ) combined with the larger equivalent sharp radius  $R$  in the  $0^\circ$  direction finally leads to a smaller  $\Delta R_{\text{np}}^{\text{surf}}$  in this direction. In the  $90^\circ$  direction, the situation is the opposite. All those results are consistent with the conclusions drawn from Fig. 9.

## V. SUMMARY

An accurate determination of the neutron skin thickness in finite nuclei provides crucial constraints on the density dependence of the nuclear symmetry energy, which further plays an indispensable role in nuclear physics and astrophysics. As the continue of our previous work for the transuranic Bk isotopes in Ref. [34] this work presents a systematic investigation of neutron skin thickness  $\Delta R_{\text{np}}$  based on the deformed relativistic Hartree-Bogoliubov theory in continuum (DRHBc). For the first time the relative contributions of the volume and surface terms are examined for deformed nuclei, and the anisotropy in neutron skin thickness and in these contributions are disclosed.

Firstly, the rms radii for neutrons and protons as well as the neutron skin thickness directly from DRHBc calculations are analyzed. The rms radii both for neutrons and protons generally increase with  $N$ , with noticeable kinks at the neutron magic numbers  $N = 184$  and  $N = 258$ . Similarly, the neutron skin thickness also increases with  $N$  but exhibits anti-kinks at neutron shell closures. Besides, when comparing with the spherical RCHB results, obvious deformation effect has been suggested to extent the nuclear spatial distributions as well as the neutron skin thickness.

Subsequently, the neutron skin thickness is decomposed into volume and surface terms with the 2pF parameters fitted by DRHBc densities averaged over angles. It is observed that the volume term dominates  $\Delta R_{\text{np}}$  as much as 68% in most nuclei while the surface term dominates only around the proton drip line with  $N < 142$ . Besides, the deformation effect is quantified by comparing with the results based on the spherical RCHB theory. We found that the deformation reduces the central radius  $R_c$  and the central density  $\rho_0$  slightly while enhancing the diffusion coefficient  $a$  significantly. As a result, the neutron skin thickness is obviously increased due to the deformation effect with the mainly contribution from the surface term.

Finally, the anisotropy of the neutron skin thickness has been explored along different directions, with the 2pF parameters extracted from DRHBc density distributions along the symmetry axis ( $z$ ,  $\theta = 0^\circ$ ) and perpendicular to it ( $r_\perp$ ,  $\theta = 90^\circ$ ), respectively. A strong directional dependence is observed for neutron skin thickness in prolate deformed nuclei, although they are elongated along the symmetry axis  $z$ , the  $\Delta R_{\text{np}}$  perpendicular to the symmetry axis ( $\theta = 90^\circ$ ) is significantly larger than that along the symmetry axis  $\theta = 0^\circ$ . In contrast, for nuclei in oblate shapes near the magic closures  $N = 184, 258$ , this anisotropy is weak. Besides, the anisotropy of the neutron skin thickness is mainly due to the volume term, which remains the dominant contribution to  $\Delta R_{\text{np}}$  in most nuclei, regardless of the direction.

### Acknowledgments

Helpful discussions with members of the DRHBc Mass Table Collaboration are highly appreciated. This work was partly supported by the Natural Science Founda-

tion of Henan Province (No. 242300421156), the National Natural Science Foundation of China (No. 12481540215, No. U2032141, and No. 12435006), National Key R&D Program of China (No. 2024YFE0109803), and the Fundamental Research Funds for the Central Universities.

- 
- [1] X. Viñas, M. Centelles, X. Roca-Maza, and M. Warda, *Eur. Phys. J. A* **50**, 27 (2014).
- [2] D. Q. Fang, *Nucl. Tech.* **46**, 080016 (2023).
- [3] M. Q. Ding, D. Q. Fan, and Y. G. Ma, *Nucl. Sci. Tech.* **35**, 211 (2024).
- [4] J. M. Mammei, C. J. Horowitz, J. Piekarewicz, B. T. Reed, and C. Sfiенти, *Annu. Rev. Nucl. Part. Sci.* **74**, 321 (2024).
- [5] B. Alex Brown, *Phys. Rev. Lett.* **85**, 5296 (2000).
- [6] R. Furnstahl, *Nucl. Phys. A* **706**, 85 (2002).
- [7] A. W. Steiner, M. Prakash, J. M. Lattimer, and P. J. Ellis, *Phys. Rep.* **411**, 325 (2005).
- [8] B. G. Todd-Rutel and J. Piekarewicz, *Phys. Rev. Lett.* **95**, 122501 (2005).
- [9] M. Centelles, X. Roca-Maza, X. Viñas, and M. Warda, *Phys. Rev. Lett.* **102**, 122502 (2009).
- [10] A. Carbone, G. Colò, A. Bracco, L. G. Cao, P. F. Bortignon, F. Camera, and O. Wieland, *Phys. Rev. C* **81**, 041301 (2010).
- [11] L. W. Chen, C. M. Ko, B. A. Li, and J. Xu, *Phys. Rev. C* **82**, 024321 (2010).
- [12] M. B. Tsang, Y. Zhang, P. Danielewicz, M. Famiano, Z. Li, W. G. Lynch, and A. W. Steiner, *Phys. Rev. Lett.* **102**, 122701 (2009).
- [13] X. Roca-Maza, M. Centelles, X. Viñas, and M. Warda, *Phys. Rev. Lett.* **106**, 252501 (2011).
- [14] B. A. Li, L. W. Chen, and C. M. Ko, *Phys. Rep.* **464**, 113 (2008).
- [15] J. Xu, L. W. Chen, B. A. Li, and H. R. Ma, *Astr. J.* **697**, 1549 (2009).
- [16] B. J. Cai, B. A. Li, and L. W. Chen, *Phys. Rev. C* **94**, 061302 (2016).
- [17] W. M. Guo, B. A. Li, and G. C. Yong, *Phys. Rev. C* **108**, 034617 (2023).
- [18] A. W. Steiner and A. L. Watts, *Phys. Rev. Lett.* **103**, 181101 (2009).
- [19] D. H. Wen, B. A. Li, and P. G. Krastev, *Phys. Rev. C* **80**, 025801 (2009).
- [20] T.-T. Sun, C.-J. Xia, S.-S. Zhang, and M. S. Smith, *Chin. Phys. C* **42**, 025101 (2018).
- [21] T.-T. Sun, S.-S. Zhang, Q.-L. Zhang, and C.-J. Xia, *Phys. Rev. D* **99**, 023004 (2019).
- [22] C.-J. Xia, H.-M. Jin, and T.-T. Sun, *Phys. Rev. D* **108**, 054013 (2023).
- [23] I. Angeli, *At. Data Nucl. Data Tables* **87**, 185 (2004).
- [24] G. W. Hoffmann, L. Ray, and M. L. Barlett, *Phys. Rev. Lett.* **47**, 1436 (1981).
- [25] V. E. Starodubsky and N. M. Hintz, *Phys. Rev. C* **49**, 2118 (1994).
- [26] A. Trzcińska, J. Jastrzębski, P. Lubiński, F. J. Hartmann, R. Schmidt, T. von Egidy, and B. Kłos, *Phys. Rev. Lett.* **87**, 082501 (2001).
- [27] T. Donnelly, J. Dubach, and I. Sick, *Nucl. Phys. A* **503**, 589 (1989).
- [28] C. J. Horowitz, *Phys. Rev. C* **47**, 826 (1993).
- [29] A. Krasznahorkay, J. Bacelar, J. Bordewijk, et al., *Phys. Rev. Lett.* **66**, 1287 (1991).
- [30] A. Krasznahorkay, M. Fujiwara, and P. van Aarle, *Phys. Rev. Lett.* **82**, 3216 (1999).
- [31] M. Warda, X. Viñas, X. Roca-Maza, and M. Centelles, *Phys. Rev. C* **81**, 054309 (2010).
- [32] M. Centelles, X. Roca-Maza, X. Viñas, and M. Warda, *Phys. Rev. C* **82**, 054314 (2010).
- [33] D. Adhikari, H. Albatineh, and D. Androic, *Phys. Rev. Lett.* **126**, 172502 (2021).
- [34] Z. D. Huang, W. Zhang, S. Q. Zhang, and T. T. Sun, *Phys. Rev. C* **111**, 034314 (2025).
- [35] S. G. Zhou, J. Meng, P. Ring, and E. G. Zhao, *Phys. Rev. C* **82**, 011301 (2010).
- [36] L. L. Li, J. Meng, P. Ring, E. G. Zhao, and S. G. Zhou, *Phys. Rev. C* **85**, 024312 (2012).
- [37] L. L. Li, J. Meng, P. Ring, E. G. Zhao, and S. G. Zhou, *Chin. Phys. Lett.* **29**, 042101 (2012).
- [38] K. Y. Zhang, M. K. Cheoun, Y. B. Choi, et al., (DRHBc Mass Table Collaboration), *Phys. Rev. C* **102**, 024314 (2020).
- [39] C. Pan, M. K. Cheoun, Y. B. Choi, et al., (DRHBc Mass Table Collaboration), *Phys. Rev. C* **106**, 014316 (2022).
- [40] K. Y. Zhang, M. K. Cheoun, Y. B. Choi, et al., (DRHBc Mass Table Collaboration), *At. Data Nucl. Data Tables* **144**, 101488 (2022).
- [41] P. Guo et al., (DRHBc Mass Table Collaboration), *At. Data Nucl. Data Tables* **158**, 101661 (2024).
- [42] K. Y. Zhang, C. Pan, S. Q. Zhang, and J. Meng, *Chin. Sci. Bull.* **66**, 3561 (2021).
- [43] K. Y. Zhang, P. Papakonstantinou, M. H. Mun, Y. Kim, H. Yan, and X. X. Sun, *Phys. Rev. C* **107**, L041303 (2023).
- [44] R. Y. Zheng, X. X. Sun, G. F. Shen, and L. S. Geng, *Chin. Phys. C* **48**, 014107 (2024).
- [45] Y. X. Zhang, B. R. Liu, K. Y. Zhang, and J. M. Yao, *Phys. Rev. C* **110**, 024302 (2024).
- [46] K. Y. Zhang, C. Pan, and X. H. Wu, *Phys. Rev. C* **112**, L051303 (2025).
- [47] E. J. In, P. Papakonstantinou, Y. Kim, and S. W. Hong, *Int. J. Mod. Phys. E* **30**, 2150009 (2021).
- [48] X. T. He, C. Wang, K. Y. Zhang, and C. W. Shen, *Chin. Phys. C* **45**, 101001 (2021).
- [49] C. Pan, K. Y. Zhang, P. S. Chong, C. Heo, M. C. Ho, J. Lee, Z. P. Li, W. Sun, C. K. Tam, S. H. Wong, et al., *Phys. Rev. C* **104**, 024331 (2021).
- [50] K. Y. Zhang, X. T. He, J. Meng, C. Pan, C. W. Shen, C. Wang, and S. Q. Zhang, *Phys. Rev. C* **104**, L021301 (2021).
- [51] X.-T. He, J.-W. Wu, K.-Y. Zhang, and C.-W. Shen, *Phys. Rev. C* **110**, 014301 (2024).
- [52] M. H. Mun, E. Ha, M. K. Cheoun, Y. Tanimura, H. Sagawa, and G. Colò, *Phys. Rev. C* **111**, 054305

- (2025).
- [53] Y. Xiao, S. Z. Xu, R. Y. Zheng, X. X. Sun, L. S. Geng, and S. S. Zhang, *Phys. Lett. B* **845**, 138160 (2023).
- [54] M.-H. Mun, K. Heo, and M.-K. Cheoun, *Particles* **8**, 42 (2025).
- [55] Y. B. Choi, C. H. Lee, M. H. Mun, S. Choi, and Y. Kim, *Phys. Rev. C* **109**, 054310 (2024).
- [56] S. Kim, M. H. Mun, M.-K. Cheoun, and E. Ha, *Phys. Rev. C* **105**, 034340 (2022).
- [57] X. Y. Zhang, Z. M. Niu, W. Sun, and X. W. Xia, *Phys. Rev. C* **108**, 024310 (2023).
- [58] M. H. Mun, S. Kim, M. K. Cheoun, W. Y. So, S. Choi, and E. Ha, *Phys. Lett. B* **847**, 138298 (2023).
- [59] C. Pan and J. Meng, *Phys. Rev. C* **112**, 024316 (2025).
- [60] M. H. Mun, E. Ha, Y. B. Choi, and M. K. Cheoun, *Phys. Rev. C* **110**, 024310 (2024).
- [61] M. H. Mun, P. Papakonstantinou, and Y. Kim, *Particles* **8**, 32 (2025).
- [62] E. J. In, Y. Kim, P. Papakonstantinou, and S.-W. Hong, *J. Korean Phys. Soc.* **77**, 966 (2020).
- [63] P. Guo, C. Pan, Y. C. Zhao, X. K. Du, and S. Q. Zhang, *Phys. Rev. C* **108**, 014319 (2023).
- [64] Y. B. Choi, C. H. Lee, M. W. Mun, and Y. Kim, *Phys. Rev. C* **105**, 024306 (2022).
- [65] W. Zhang, J. K. Huang, T.-T. Sun, J. Peng, and S. Q. Zhang, *Chin. Phys. C* **48**, 104105 (2024).
- [66] C. Zhou, P. Guo, and X. F. Jiang, *Particles* **7**, 1128 (2024).
- [67] X. X. Sun, *Phys. Rev. C* **103**, 054315 (2021).
- [68] C. Pan, K. Y. Zhang, and S. Q. Zhang, *Phys. Lett. B* **855**, 138792 (2024).
- [69] X. X. Sun and S. G. Zhou, *Nucl. Phys. Rev.* **41**, 75 (2024).
- [70] X. X. Sun and S. G. Zhou, *Sci. Bull.* **66**, 2072–2078 (2021).
- [71] K. Y. Zhang, S. Q. Zhang, and J. Meng, *Phys. Rev. C* **108**, L041301 (2023).
- [72] K. Y. Zhang, S. Q. Yang, J. L. An, S. S. Zhang, P. Papakonstantinou, M.-H. Mun, Y. Kim, and H. Yan, *Phys. Lett. B* **844**, 138112 (2023).
- [73] J. L. An, K. Y. Zhang, Q. Lu, S. Y. Zhong, and S. S. Zhang, *Phys. Lett. B* **849**, 138422 (2024).
- [74] P. W. Zhao, Z. P. Li, J. M. Yao, and J. Meng, *Phys. Rev. C* **82**, 054319 (2010).
- [75] X. H. Wu, C. Pan, K. Y. Zhang, and J. Hu, *Phys. Rev. C* **109**, 024310 (2024).
- [76] K. Y. Zhang, C. Pan, X. H. Wu, X. Y. Qu, X. X. Lu, and G. A. Sun, *AAPPS Bull.* **35**, 13 (2025).
- [77] X. Y. Qu, K. M. Chen, C. Pan, Y. Y. Yu, and K. Y. Zhang, *Nucl. Sci. Tech.* **36**, 231 (2025).
- [78] X. W. Xia, Y. Lim, P. W. Zhao, et al., *At. Data Nucl. Data Tables* **121**, 1 (2018).
- [79] C. E. Price and G. E. Walker, *Phys. Rev. C* **36**, 354 (1987).
- [80] R. W. Hasse and W. D. Myers, *Geometrical Relationships of Macroscopic Nuclear Physics* (Springer-Verlag, Heidelberg, 1988).
- [81] G. Süßmann, *Z. Phys. A* **274**, 145 (1975).
- [82] S. G. Zhou, J. Meng, and P. Ring, *Phys. Rev. C* **68**, 034323 (2003).
- [83] K. Y. Zhang, C. Pan, and S. Q. Zhang, *Phys. Rev. C* **106**, 024302 (2022).
- [84] C. Pan, K. Y. Zhang, and S. Q. Zhang, *Int. J. Mod. Phys. E* **28**, 1950082 (2019).